JOURNAL OF COMPUTATIONAL PHYSICS 60, 376–390 (1985)

Computation of Hele–Shaw Flows with Free Boundaries

JOYCE M. AITCHISON*

Oxford University Computing Laboratory, 19 Parks Road, Oxford OX1 3PL, United Kingdom

AND

S. D. HOWISON

Mathematical Institute, 24–29 St Giles, Oxford OX1 3LB, United Kingdom

Received July 27, 1983; revised November 16, 1984

A novel method for calculation of Hele–Shaw flows with receding free boundaries is presented. The method is applied to flows with suction from a point sink and to flow in a channel with parallel walls. In each case the unknown fluid region is mapped conformally onto the unit disc, the free boundary being mapped onto the unit circle. This mapping, which is a function of position and time, is calculated numerically at points on the unit circle using a version of the boundary integral method. The free boundary is thus found without explicit calculation of the pressure at internal points, and the computation times are much less than those for other numerical methods for this problem. Numerical results are compared with explicit analytic solutions for several test problems.

1. INTRODUCTION

This paper is concerned with the numerical solution of some time-dependent free boundary problems arising from flow of an incompressible viscous fluid in a Hele–Shaw cell, which consists of two parallel horizontal plates separated by a thin gap. A blob of fluid is forced to move in this gap by sources or sinks within the fluid, or by injection or extraction at the edges of the cell. For slow flow in a thin gap, the flow is approximately two-dimensional, and with suitable scaling the fluid velocity $\mathbf{q}$ is given in cartesian coordinates by

$$\mathbf{q} = (u, v) = -\nabla p, \tag{1.1}$$

where p is the pressure; the equation of continuity then gives

$$\nabla^2 p = 0 \tag{1.2}$$

* Present address: Mathematics and Ballistics Group, Royal Military College of Science, Shrivenham, Swindon SN6 8LA, United Kingdom.

0021-9991/85 $3.00

in the fluid region $\Omega(t)$. We shall ignore surface tension effects [17], and assume that the pressure is constant at the fluid–air interface $\partial\Omega(t)$; this constant may be taken equal to zero. The second condition applying on $\partial\Omega(t)$ is that the material derivative of p vanishes since p is constant there, so

$$p=0, \qquad \frac{\partial p}{\partial t}-\nabla p\cdot\nabla p=0 \text{ on } \partial\Omega(t). \tag{1.3}$$

In this paper we shall only consider flows with a single point source or sink, and flow in a channel with parallel walls $y=\pm\pi$ with uniform suction at infinity. In the former case, if the sink is of strength Q and is at (x_0, y_0), then near this point

$$p\sim -\frac{Q}{2\pi}\ln((x-x_0)^2+(y-y_0)^2)^{1/2}, \tag{1.4a}$$

while for flow in a channel

$$p\sim -Vx \qquad \text{as } x\to\infty, \tag{1.4b}$$

where the extraction rate is $2\pi V$, and the fluid velocity tends to $(V, 0)$ as $x\to\infty$. Finally, we shall assume that $\partial\Omega(0)$ is a given analytic curve.

In addition to describing Hele–Shaw flow, the problem of Eqs. (1.1)–(1.4) also models two-dimensional flow in a porous medium under D'Arcy's law [2], and a process in electro-chemical machining [9].

If in Eq. (1.4), $Q>0$ (so that there is injection of fluid at (x_0, y_0)), the free boundary problem of Eqs. (1.1)–(1.4a) can be shown to be well-posed [4], and computation of the free boundary $\partial\Omega(t)$ presents no difficulties [5]. However, when fluid is extracted ($Q<0$), the behaviour of the solution is in general quite different. The free boundary is now receding, and a local linear stability analysis shows that small perturbations with wavelength $2\pi/n$ of a free boundary receding with speed V have a growth rate $e^{|n|Vt}$, [17]. The free boundary is thus unstable to perturbations of all wavelengths, with the shortest wavelength disturbances growing the fastest. A global, nonlinear analysis (see Sect. 2 and [7]) reveals that almost all receding Hele–Shaw flows break down in finite time or before all the fluid has been extracted. This breakdown consists of the formation of a cusp in the free boundary, at which the model predicts infinite fluid velocities, and for a given analytic curve $\partial\Omega(0)$ there are solutions which start with their initial curve arbitrarily close to $\partial\Omega(0)$ and which blow up in an arbitrarily short time.

Numerical calculation of receding Hele–Shaw problems therefore presents formidable difficulties. Of the two types of problems we consider here, we may achieve reasonable results with flow in a finite blob, provided that the exact solution for the given initial curve does not exist for too long; but it is inevitable that computation of flow in channels will eventually break down, and we do not therefore expect to be able to reproduce solutions such as the Saffman–Taylor "fingers" (Section 2) over large time intervals. One of the results of interest in this work, therefore, is the

timescale over which successful reproduction of receding Hele–Shaw flows is possible before numerical instabilities cause the numerical solution to break down.

Recent work in this field has been described by Meng and Thomson in [10] and by Meyer in [12]; there are also numerical solutions for steadily progressing channel flow in [8, 15]. Meng and Thomson use a vortex element method based on a line distribution of vorticity on the free boundary; however, they provide no quantitative comparison with explicit solutions, and they do not mention the possibility of cusp development. Meyer uses the method of invariant embedding to solve Eqs. (1.1)–(1.4a) for a shape which is initially a limaçon containing a point sink (represented by a small circle surrounding the origin on which the pressure is a large negative constant). This solution develops a cusp before all the fluid has been extracted; we shall discuss it further below, in Sections 2 and 3. Here we merely remark that although the method of [12] is accurate it is also expensive in computer time, because the iterative scheme used is slow and because the method used calculates the pressure at all internal mesh points. In general, it is only of interest to know the free boundary $\partial\Omega(t)$; consequently, any method which computes only the free boundary, without the expense of computing the interior pressures, is desirable. In Section 2 we use conformal mapping to transform the moving boundary problem to one in a fixed domain, in this case a circle (similar techniques have been used in [11] to find numerical solutions to the Rayleigh–Taylor problem). For our particular problem, this results in a considerable saving of computational cost. The transformed problem is solved using a boundary integral method which proves to be well suited to a circular geometry. This numerical method is illustrated by comparison with the explicit solutions to be presented in Section 2.

2. Application of Complex Variable Theory

Since the pressure p is harmonic, the complex potential $w(z, t) = -(p + i\psi)$, where $z = x + iy$ and ψ is the harmonic conjugate of p, is analytic for all z in $\Omega(t)$ except at a point sink at, say, $z = z_0$, near which $w(z) \sim Q/2\pi \ln(z - z_0)$. Condition (1.3) thus becomes

$$\mathrm{Re}(w) = 0, \tag{2.1a}$$

$$\mathrm{Re}\left(\frac{\partial w}{\partial t}\right) = -\left|\frac{\partial w}{\partial z}\right|^2 \tag{2.1b}$$

for $z \in \partial\Omega(t)$.

Because $\Omega(t)$ is unknown for $t > 0$, it is not easy to solve directly for $w(z, t)$. Instead, we map $\Omega(t)$ conformally onto a known, fixed region in which the complex potential is easily calculated; we then use condition (2.1b) to formulate a problem for the unknown mapping function in this fixed domain.

Following [14], let us map $\Omega(t)$ onto the unit disc by

$$z = f(\zeta, t), \tag{2.2}$$

where f is conformal for $|\zeta| < 1$; *i.e.*, f is analytic and $df/d\zeta \neq 0$. The Riemann mapping theorem guarantees the existence of such a function whenever $\Omega(t)$ is finite and simply connected, and we may specify the image of one point and of one direction through that point [13]. We use these conditions to require that $f(0, t) = 0$ and that the directions of the real z and real ζ axes should coincide at their respective origins. We can now immediately write down the complex potential in the ζ plane: this is $W(\zeta) = (Q/2\pi) \ln \zeta$, and using the fact that $\partial\zeta/\partial t = -(\partial f/\partial t)/(df/d\zeta)$, we have $\partial w/\partial t = -Q(\partial f/\partial t)/(2\pi\, df/d\zeta)$, so that after clearing $|df/d\zeta|^2$ from both sides, (2.1b) becomes

$$\mathrm{Re}\left(\zeta \frac{df}{d\zeta}\overline{\frac{\partial f}{\partial t}}\right) = \frac{Q}{2\pi} \qquad \text{on } |\zeta| = 1. \tag{2.3}$$

Given $\Omega(0)$, we therefore have to find a function $f(\zeta, t)$ such that

(i) $f(\zeta, t)$ is analytic in $|\zeta| < 1$, $t \geqslant 0$,

(ii) $f'(\zeta, t) \neq 0$ in $|\zeta| < 1$, $t \geqslant 0$,

(iii) $f(0, t) = 0$, $f'(0, t)$ is real and positive, $t \geqslant 0$, (2.4)

(iv) The image of $|\zeta| < 1$ under $f(\zeta,0)$ is $\Omega(0)$,

(v) $\mathrm{Re}(\zeta(df/d\zeta)(\overline{\partial f/\partial t})) = Q/2\pi$ on $|\zeta| = 1$, $t > 0$.

We remark here that cusp formation corresponds to the situation where a zero of $df/d\zeta$ (which at $t = 0$ must lie outside $|\zeta| = 1$) reaches $|\zeta| = 1$; (2.3) then shows that $|\partial f/\partial t|$ is infinite at that point. We shall later approximate $\partial\Omega(t)$ by straight lines joining the images of 2N points equally spaced around $|\zeta| = 1$. Since the local scaling of the map (2.2) is $|df/d\zeta|$, the images of points on $|\zeta| = 1$ near to a zero of $df/d\zeta$ (and so where $\partial\Omega(t)$ has high curvature) are relatively close together, and $\partial\Omega(t)$ is thus represented most accurately where it is most highly curved.

We shall discuss here the example treated in [12],

$$z = a_1(t)\,\zeta + a_2(t)\,\zeta^2, \tag{2.5}$$

where, from (2.3), we obtain $a_1^2 + 2a_2^2 = (Qt/\pi) + \alpha^2 + 2\beta^2$, $a_1^2 a_2 = \alpha^2\beta$, where $a_1(0) = \alpha$, $a_2(0) = \beta$, and $4\beta^2 < \alpha^2$. There is a zero of $dz/d\zeta$ at $\zeta = -a_1/2a_2$ which reaches $|\zeta| = 1$ when $a_1^2 = 4a_2^2$, at time $t = t_{\mathrm{crit}} = (\pi/Q)(6(\alpha^2\beta/4)^{2/3} - \alpha^2 - 2\beta^2)$, and at this stage the free boundary develops a cusp (see Fig. 2).

The second class of flow we describe is flow in a channel with walls $y = \pm\pi$. We shall consider only flows which are symmetrical about the centerline $y = 0$. Once again we map $\Omega(t)$ conformally onto the unit disc $|\zeta| < 1$, but since $\Omega(t)$ now extends to infinity in the positive x-direction, we write

$$z = -\ln \zeta + h(\zeta, t), \tag{2.6}$$

where $h(\zeta, t)$ is analytic in $|\zeta| < 1$, h is real on the negative real axis, and the principal branch of the logarithm is taken. The complex potential is now $-V \ln \zeta$, and we find [7] that h must satisfy

$$\begin{aligned} &\text{(i)} \quad h(\zeta, t) \text{ analytic in } |\zeta| < 1,\ t \geqslant 0, \\ &\text{(ii)} \quad -1/\zeta + (dh/d\zeta) \neq 0 \text{ in } |\zeta| < 1,\ t \geqslant 0, \\ &\text{(iii)} \quad h(\zeta, 0) \text{ is known}, \\ &\text{(iv)} \quad \mathrm{Re}((\zeta dh/d\zeta - 1)\,\overline{\partial h/\partial t}) = -V \text{ on } |\zeta| = 1. \end{aligned} \tag{2.7}$$

Note that it is not necessary to specify $h(0, t)$.

We shall discuss in particular two examples. First, when

$$z = -\ln \zeta + b_0(t) + b_1(t)\,\zeta, \tag{2.8}$$

we find that $b_0 - \frac{1}{2}b_1^2 = Vt - \frac{1}{2}\varepsilon^2$, $b_1 e^{-b_0} = \varepsilon$, where $b_0(0) = 0$ and $b_1(0) = \varepsilon (0 \leqslant \varepsilon < 1)$. If ε is small, at $t = 0$ the free boundary consists of a small perturbation of a planar boundary; it can be written $x \sim \varepsilon \cos y + 0(\varepsilon^2)$. However, as t increases, this perturbation grows, until at $t = t_{\mathrm{crit}} = (1/V)(\varepsilon^2/2 - \frac{1}{2} + \ln(1/\varepsilon))$ a cusp forms (Fig. 3); once again this is caused by a zero of $dz/d\zeta$ reaching $|\zeta| = 1$.

Our second example is discussed in [16]. Here, we take

$$z = -\ln \zeta + d(t) + 2(1 - \lambda) \ln(1 + a(t)\zeta), \tag{2.9}$$

where

$$a(0) = \varepsilon \ (0 \leqslant \varepsilon < 1),\ (a/\varepsilon)((1 - a^2)/(1 - \varepsilon^2))^{-2\lambda(1-\lambda)} = e^{Vt},$$

$d(t) = Vt - 2(1 - \lambda)^2 \ln((1 - a^2)/(1 - \varepsilon^2))$, and λ is an arbitrary parameter with $0 < \lambda < 1$. If $\varepsilon \ll 1$, at $t = 0$ this solution also has a free boundary which has the form $x \sim \varepsilon \cos y + 0(\varepsilon^2)$. However, the solution does not break down; instead the perturbation grows until for large values of t it forms a steadily progressing "finger" occupying a fraction λ of the channel and moving with speed $U = V/\lambda$, (Fig. 1).

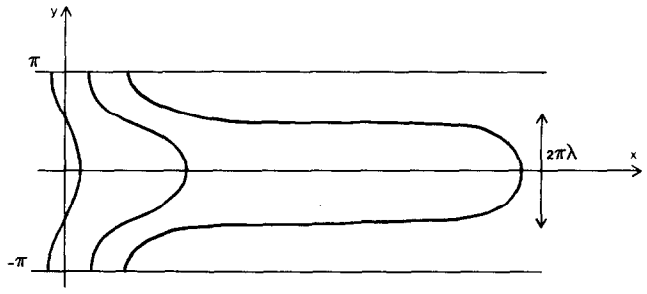

FIG. 1. Sketch of the development of a Saffman finger (Eq. (2.9)).

3. Numerical Solution

We first consider flow with a point sink at the origin. Equation (2.4) can be rewritten as a pair of partial differential equations as follows. Define polar coordinates ρ, θ so that $\zeta = \rho e^{i\theta}$, and let $f(\zeta, t) = f_1(\rho, \theta, t) + if_2(\rho, \theta, t)$, where f_1 and f_2 are real functions which are harmonic in $\rho < 1$ and satisfy the Cauchy–Riemann equations

$$\frac{\partial f_1}{\partial \rho} = \frac{1}{\rho}\frac{\partial f_2}{\partial \theta}, \qquad \frac{\partial f_2}{\partial \rho} = -\frac{1}{\rho}\frac{\partial f_1}{\partial \theta}.$$

Condition (2.4v) may then be written

$$\frac{\partial f_1}{\partial \rho}\frac{\partial f_1}{\partial t} + \frac{\partial f_2}{\partial \rho}\frac{\partial f_2}{\partial t} = \frac{Q}{2\pi} \qquad \text{on } \rho = 1. \tag{3.1}$$

We also have, from (2.4iii), that

$$\int_0^{2\pi} f_1(1, \theta, t)\, d\theta = \int_0^{2\pi} f_2(1, \theta, t)\, d\theta = 0, \qquad t \geqslant 0.$$

We calculate f_1 and f_2 at a series of time levels $t = n\,\Delta t$, $n = 1,2,\ldots$. The time derivative in the boundary condition (3.1) is approximated by an explicit difference, and we find the following set of equations to be solved for $f_1^{(n)}$ and $f_2^{(n)}$, the values of f_1 and f_2 at $t = n\,\Delta t$:

$$\nabla^2 f_1^{(n)} = 0, \tag{3.2a}$$

$$\nabla^2 f_2^{(n)} = 0 \qquad \text{in } \rho < 1, \tag{3.2b}$$

with boundary conditions on $\rho = 1$, $n > 0$,

$$\frac{\partial f_2^{(n)}}{\partial \theta} = \frac{\partial f_1^{(n)}}{\partial \rho} \tag{3.3}$$

$$\left(\frac{f_1^{(n)} - f_1^{(n-1)}}{\Delta t}\right)\frac{\partial f_1^{(n-1)}}{\partial \rho} + \left(\frac{f_2^{(n)} - f_2^{(n-1)}}{\Delta t}\right)\frac{\partial f_2^{(n-1)}}{\partial \rho} = \frac{Q}{2\pi}, \tag{3.4}$$

and with the subsidiary conditions

$$\int_0^{2\pi} f_1^{(n)}(1, \theta)\, d\theta = 0 \tag{3.5}$$

$$\int_0^{2\pi} f_2^{(n)}(1, \theta)\, d\theta = 0. \tag{3.6}$$

For $n \geqslant 1$ we calculate $f_1^{(n)}$ and $f_2^{(n)}$ using known values of $f_1^{(n-1)}$ and $f_2^{(n-1)}$. For $n = 0$, Eq. (3.4) is replaced by an initial condition

$$f_1^{(0)} = g(\theta) \qquad \text{on } \rho = 1, \tag{3.7}$$

where g is the real part of $f(e^{i\theta}, 0)$, and is assumed known. For a known initial fluid region $\Omega(0)$, g may be computed numerically by, for example, Theodorsen's method [6].

As stated above, the values of f_1 and f_2 which are of interest are those on the boundary $\rho = 1$ of the solution region, and so we use a boundary element method to obtain an approximate solution to Eq. (3.2). This method is becoming more widely known, and descriptions can be found in [1]. The present problem differs from previous applications of the boundary element technique in two ways: first we have an unusual set of boundary conditions, the effect of which will be discussed later, and second the solution is to be obtained on a circular region, whereas the method is normally applied to polygonal regions, or polygonal approximations of other regions. We will first describe the modifications of the standard method due to the circular region.

Let Φ be an unknown function harmonic in $\rho < 1$, and let ζ_0 be a point on $\rho = 1$. Then we can use Green's theorem to show that

$$\pi\Phi(\zeta_0) = \int_C \left(\Phi \frac{\partial \psi}{\partial \rho} - \psi \frac{\partial \Phi}{\partial \rho} \right) d\theta \tag{3.8}$$

where C is the circle $\rho = 1$, and $\psi(\zeta; \zeta_0) = \ln|\zeta - \zeta_0|$. Now ζ and ζ_0 both lie on $\rho = 1$, so writing $\zeta = e^{i\theta}$, $\zeta_0 = e^{i\theta_0}$, we obtain

$$\psi(\zeta; \zeta_0) = \ln|2 \sin \tfrac{1}{2}(\theta - \theta_0)|,$$

and furthermore the normal derivative of ψ has the particularly simple form $\partial\Psi/\partial\rho = \frac{1}{2}$. The circle C is divided into elemental arcs and Φ and $\partial\Phi/\partial\rho$ are approximated by simple functions on each element in terms of nodal values. Equation (3.8) is now applied at each nodal point as in the conventional boundary element technique.

We will now describe the solution of Eqs. (3.2)–(3.6) using piecewise linear elements. All the problems considered in this paper are symmetric about the line $\theta = 0$; i.e., $f_1(\rho, 2\pi - \theta, t) = f_1(\rho, \theta, t)$, $f_2(\rho, 2\pi - \theta, t) = -f_2(\rho, \theta, t)$, and so we only consider the half circle $0 \leqslant \theta \leqslant \pi$. This is divided into N equal arcs, $k\,\Delta\theta < \theta < (k+1)\Delta\theta$ for $k = 0, 1, \ldots, N-1$, where $\Delta\theta = \pi/N$, and nodal points are taken at $\theta = \theta_k = k\,\Delta\theta$, $k = 0, \ldots, N$. Let $f_{ik}^{(n)}$ be the approximate value of $f_1^{(n)}$ at $\rho = 1$, $\theta = \theta_k$, and similarly let $f_{2k}^{(n)}, f_{ik}^{(n)'}$, and $f_{2k}^{(n)'}$ be the corresponding values of $f_2^{(n)}$, $\partial f_1^{(n)}/\partial\rho$, and $\partial f_2^{(n)}/\partial\rho$. The application of (3.8) with Φ replaced by $f_1^{(n)}$ gives a set of $(N+1)$ linear equations relating $\{f_{1k}^{(n)}\}$ and $\{f_1^{(n)'}\}$ for $k = 0, \ldots, N$, which is effectively the numerical solution of Eq. (3.2a). Similarly Eq. (3.2b) yields a further

$(N+1)$ equations relating $\{f_{2k}^{(n)}\}$ and $\{f_{2k}^{(n)'}\}$. The Cauchy–Riemann equation (3.3) is discretized on the k*th* element as

$$(f_{2k}^{(n)} - f_{2,k-1}^{(n)})/\Delta\theta = \tfrac{1}{2}(f_{1k}^{(n)'} + f_{1,k-1}^{(n)'}), \qquad k = 1, 2, ..., N.$$

The orientation of the mapping can be fixed by imposing

$$f_{2,0}^{(n)} = 0.$$

We now have $3(N+1)$ equations relating the $4(N+1)$ unknowns. When $n=0$ the remaining $(N+1)$ equations come from applying (3.7) at $\theta = \theta_k$, $k = 0, ..., N$, while for $n > 0$, they are provided by Eq. (3.4).

The subsidiary conditions in Eqs. (3.5) and (3.6) have not so far been considered. Condition (3.6) is automatically satisfied once symmetry has been assumed but condition (3.5) will not necessarily be satisfied. However, in practise, we observe that the algebraic system derived from Eqs. (3.2)–(3.4) is nearly singular in the sense that one of the eigenvalues is much smaller than the rest; the explanation for this is as follows. The mapping $z = f(\zeta, t)$ is unique only if the image of one point is specified, and by ignoring Eq. (3.5) we are underspecifying the problem. Ideally this would be brought out by the system of linear algebraic equations becoming singular, but since these equations have been derived using approximate integration, this exact singularity has been lost. The near singularity of the algebraic system is avoided by replacing one of the Eqs. (3.4) by the approximate form of Eq. (3.5). This difficulty does not occur when $n=0$, since the initial mapping is chosen to satisfy $f(0, 0) = 0$. See the Appendix for a further discussion of this point.

The second problem which we consider is that of flow in a channel governed by Eqs. (2.7). These are again recast as partial differential equations by setting $h(\zeta, t) = h_1(\rho, \theta, t) + ih_2(\rho, \theta, t)$. Following the procedure for the previous problem we arrive at the following system:

$$\nabla^2 h_1 = 0, \qquad \nabla^2 h_2 = 0 \qquad \text{in } \rho < 1, t \geqslant 0, \tag{3.9}$$

with boundary conditions

$$\frac{\partial h_1}{\partial \rho} = \frac{\partial h_2}{\partial \theta} \qquad \text{on } \rho = 1, t \geqslant 0, \tag{3.10}$$

$$\frac{\partial h_1}{\partial t}\left(\frac{\partial h_1}{\partial \rho} - 1\right) + \frac{\partial h_2}{\partial t}\frac{\partial h_2}{\partial \rho} = -V \qquad \text{on } \rho = 1, t > 0, \tag{3.11}$$

and with $h_1(1, \theta, 0)$ given. These equations are discretized in time and then solved using boundary elements exactly as before. There are, however, no subsidiary conditions corresponding to Eqs. (3.5) and (3.6), and the algebraic system derived from the differential equations and boundary conditions is clearly non-singular (see Appendix).

We shall present results using both linear and constant approximations for f_1 and f_2 (or h_1 and h_2) on each arc. The discretization for constant elements is as straightforward as that for linear elements described above, although we remark that we have had to replace $\partial f_1/\partial\theta$ in Eq. (3.3) (and likewise in Eq. (3.10)) by a simple difference approximation. Last, in order to make comparisons with other numerical methods, we estimate our computing cost as follows. At each time step we solve a set of $4(N+1)\times 4(N+1)$ linear equations with a full matrix by a standard L–U decomposition with pivoting; this takes approximately $32N^3/3$ operations. In addition, it is worth remarking that most of the cost of assembling the matrix for these equations comes from the discretization of Eqs. (3.3) and (3.8), which depends only on the (fixed) geometry in the ζ-plane; this part of the assembly cost is thus incurred only once during the solution process.

4. Results

As a test problem for flow with a point sink, we consider the example described earlier in Eq. (2.5). We take $Q=-1$, and start with the shape given by $z=2\zeta+\frac{1}{4}\zeta^2$, for which blow-up occurs when $t=t_{\text{crit}}=5.4786$.

Table *I* shows the results of various calculations of this problem; the half circle is divided into N equal elements, and the tabulated value of t_{crit} is the last timestep before the cusp forms. The calculations were carried out using both linear and constant approximations to f_1 and f_2 on each element; these are denoted by the letters L and C.

We see from Table I that all the results are acceptable apart from those which should be most accurate, namely with $N=24$ and with linear approximations. This is a phenomenon which appears even more noticeably in our next example; it arises because we are trying to calculate a solution to a problem which is physically unstable.

As mentioned in Section 1, a physical instability of wavelength $2\pi/n$ grows at a rate proportional to $e^{|n|Vt}$, and this is reflected in the behaviour of the numerical solution (see the end of this section). By taking more elements, we permit the introduction of shorter wavelength instabilities into the numerical problem; these

TABLE I

Calculations of Blow-Up Time (Exact Value 5.4786)

N	Δt	t_{crit}	N	Δt	t_{crit}
16L	0.05	5.50	16C	0.05	5.45
16L	0.02	5.44	16C	0.02	5.40
24L	0.05	5.15	24C	0.05	5.50
24L	0.02	4.96	24C	0.02	5.46

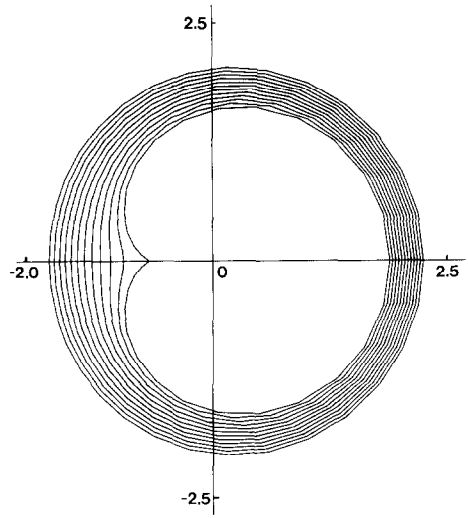

FIG. 2. Computed free boundary profiles for the cardioid problem with the sink at the origin, drawn at time intervals of 0.5.

arise from rounding errors and the approximate solution technique, and they may cause blow-up to occur earlier than the critical time which we are trying to calculate.

Figure 2 shows the result of the calculations performed with $N = 16$, $\Delta t = 0.05$ and with linear approximations; the free boundary profiles are drawn at time intervals of 0.5. It is clear from this figure that the most sensitive values of f_1 are those nearest the origin, where $\theta = \pi$. In Table II we compare the calculated values for both 16 and 24 linear elements with $t = 0.05$ against those from the exact solution of Eq. (2.5), and it is seen that the agreement is good until each solution nears its blow-up time.

TABLE II

Comparison of Exact and Computed Values of $f_1(\pi, t)$

Time t	$N = 16$	$N = 24$	Exact
1.0	1.6386	1.6389	1.6389
2.0	1.5148	1.5156	1.5155
3.0	1.3728	1.3742	1.3739
4.0	1.1996	1.2022	1.2011
5.0	0.9514	0.9542	0.9521
5.1	0.9160	0.9117	0.9162
5.15	0.8967	0.8793	0.8964
5.4	0.7692	—	0.7597
5.45	0.7294	—	0.7081
5.5	0.6720	—	—

This method has thus successfully computed the shape of the free boundary with suction. The calculations were performed on the Oxford University *ICL* 2988 machine; the complete run which produced Fig. 2 took less than 2 min. It is difficult to make exact comparisons with the computing times of Meyer [12], but our method is clearly faster, as would be expected from the argument at the end of the previous section.

We now turn our attention to the calculation of channel flow using Eqs. (3.9) and (3.11). For our first example, we set $V=1$ and take an initial shape given by eq. (2.8) as $h(\zeta, 0)=\varepsilon\zeta$. This solution was discussed in Section 2; when $\varepsilon=0.1$, it blows up when $t=t_{\text{crit}}=1.8076$. Using 16 elements on the half circle we were unable to proceed beyond $t=1.25$ with linear approximations and $t=1.63$ with constant approximations. When $\varepsilon=0.2$, the exact solution blows up for $t_{\text{crit}}=1.12924$. The results of our computation of t_{crit} in this case are shown in Table III, where in each case $\Delta t=0.01$; the letters L and C again denote linear and constant approximation respectively. (We note here that since the rate of fluid extraction is 2π, the timescale for channel flow is $1/2\pi$ times that for flow with a point sink and with $Q=-1$.)

The only one of these results which is acceptable is that which is theoretically the least accurate, namely constant approximations on 16 elements. The results of this computation are shown in Fig. 3, where the free surface profile is plotted at time intervals of 0.09.

As an example of a flow which does not produce a cusp, the method was applied with $h(\zeta, 0)=2(1-\lambda)\ln(1+\varepsilon\zeta)$, as in Eq. (2.9), with $\lambda=\frac{1}{2}$ and $\varepsilon=0.2$; the initial shape is then very similar to that in the previous calculation. Figure 4 shows the result of this calculation using constant approximations on 16 elements, and with $\Delta t=0.01$. The free surface profiles are plotted using the same time interval as that in Fig. 3, but the computation now proceeds until $t=1.26$ before instability arises (this would correspond to a time of 7.92 in flow with a point sink and $Q=-1$; the cusp in our previous example formed at $t=5.45$).

These results for channel flow illustrate the inherent instability of the problem, namely that small changes in the initial data (introduced by rounding errors, etc.) lead to large changes in the subsequent behaviour of the solution. To demonstrate this point further we consider the progress of an initially flat profile: that is, we take

TABLE III

Comparison of "Blow-Up" Times

N	t_{crit}[a]
16L	0.91
24L	0.68
16C	1.09
24C	0.85

[a] Exact value = 1.1294.

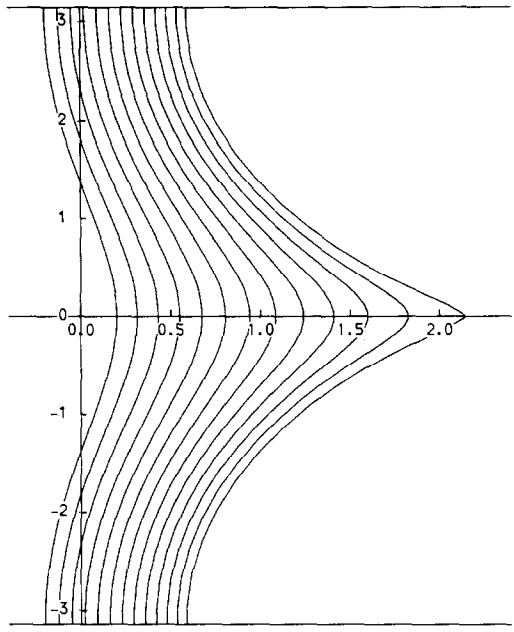

FIG. 3. Computed free boundary profiles for channel flow with initial shape given by Eq. (2.8), drawn at time intervals of 0.09.

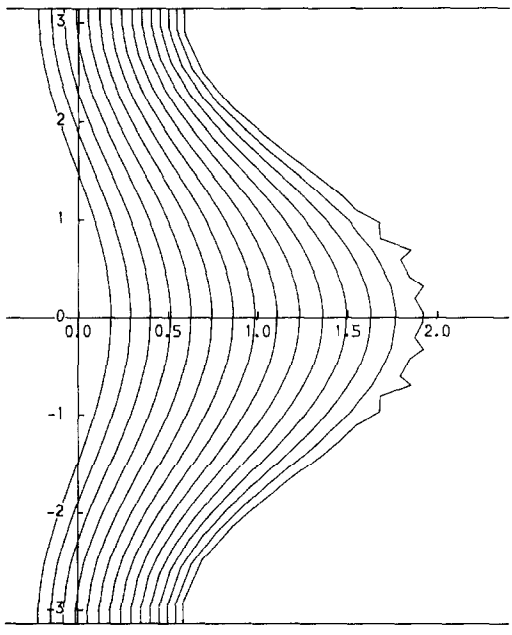

FIG. 4. Computed free boundary profiles for channel flow with initial shape given by Eq. (2.9), drawn at time intervals of 0.09.

$h(\zeta, 0) = 0$, for which the exact solution is $h(\zeta, t) = Vt$. As expected, oscillations develop in the computed free surface, and these grow with time. Using constant approximations on 16 elements and $\Delta t = 0.01$ we find that the maximum error grows by a factor of 1.86 in 5 time steps, and that the errors become $O(10^{-4})$ when $t = 2.6$. The growth factor is consistent over a long time interval and corresponds to a growth rate of $e^{12.4t}$; using linear approximations the corresponding growth rate of the maximum error is e^{17t}. Both of these growth rates agree broadly with the linear stability analysis mentioned in Section 1 if it is assumed that the shortest wavelength of the introduced errors is approximately 1/16th of channel width.

All the calculations were performed in double precision arithmetic, and so the key factor in the creation of the initial instabilities would seem to be truncation errors in the spatial discretization. Provided that the timestep is kept reasonably small (a normal condition for explicit methods), the particular timestep used has very little influence on the results. In particular, it does not affect the onset of instability, showing clearly that the instabilities observed are not induced by the numerical method, but are inherent in the mathematical problem being solved.

5. Conclusions

The method described above has worked well for the difficult problem of calculating these unstable flows. In particular it compares very favourably in terms of computing time with the method of Meyer for the calculation of flows with a point sink. As far as flow in a channel is concerned, these calculations have proceeded as far in time as any that we are aware of. However, the method is obviously limited to two-dimensional problems where a conformal mapping of the form discussed in Section 2 exists. We hope that these results show how a combination of complex variable theory and numerical methods can be used to good effect.

Appendix

We have stated that it is necessary to specify $f(0, t)$ in order that the mapping function $f(\zeta, t)$ may be uniquely determined. In this Appendix we show that if is also necessary to specify $f(0, t)$ at each timestep in the discretized problem for $f(\zeta, t)$.

Let us assume that, at the $(n-1)th$ timestep, $f(\zeta, (n-1)\,\Delta t) = f_1^{(n-1)} + if_2^{(n-1)}$ is a known analytic function of ζ satisfying (2.4). We therefore consider the problem of finding the function $f(\zeta, n\,\Delta t) = f^{(n)}(\zeta)$ which is analytic in $|\zeta| < 1$ and satisfies the boundary condition (3.4) on $|\zeta| = 1$; we shall show that the solution to this problem contains one arbitrary complex constant which can only be determined by specifying $f^{(n)}(0)$.

Noting that, on $|\zeta| = 1$, $\partial f/\partial \rho = \zeta(df/d\zeta)$, we rewrite Eq. (3.4) as

$$\mathrm{Re}\left(\zeta \frac{df^{(n)}}{d\zeta}(f^{(n)} - f^{(n-1)})\right) = \frac{Q\,\Delta t}{2\pi} \qquad \text{on } |\zeta| = 1,$$

i.e.,

$$\mathrm{Re}\left(\frac{f^{(n)} - f^{(n-1)}}{\zeta\, df^{(n-1)}/d\zeta}\right) = \frac{Q\,\Delta t}{2\pi\,|df^{(n-1)}/d\zeta|^2} \qquad \text{on } |\zeta| = 1. \tag{A.1}$$

Equation (A.1) is now a Dirichlet boundary condition for the function $(f^{(n)} - f^{(n-1)})/(\zeta\, df^{(n-1)}/d\zeta)$ which, since $df^{(n-1)}/d\zeta = 0$, is analytic in $|\zeta| < 1$ with at most a pole at $\zeta = 0$. It follows from the Poisson formula [3] that

$$f^{(n)}(\zeta, t) = f^{(n-1)}(\zeta, t) - \frac{1}{\zeta}\frac{f^{(n)}(0)}{df^{(n-1)}(0)/d\zeta} + \zeta \frac{df^{(n-1)}}{d\zeta}\left\{\frac{1}{2\pi i}\int_{|s|=1} \frac{Q\,\Delta t(s+\zeta)\;ds}{2\pi s(s-\zeta)\,|df^{(n+1)}/ds|^2} + iC_n\right\},$$

where C_n is a real constant. It can be shown that C_n must vanish if $df^{(n)}(0)/d\zeta$ is real; it is therefore clearly necessary to specify $f^{(n)}(0)$ in order that $f^{(n)}(\zeta)$ may be uniquely determined.

The corresponding procedure for channel flow, however, leads to the Dirichlet boundary condition

$$\mathrm{Re}\left[\frac{h^{(n)} - h^{(n-1)}}{\zeta dh^{(n-1)}/d\zeta - 1}\right] = \frac{-V\,\Delta t}{|\zeta dh^{(n-1)}/d\zeta - 1|^2} \tag{A.2}$$

on $|\zeta| = 1$ for the function

$$\frac{h^{(n)}(\zeta) - h^{(n-1)}(\zeta)}{\zeta dh^{(n-1)}/d\zeta - 1}.$$

Now in equation (A.1) the denominator of the left-hand side vanishes at $\zeta = 0$, leading to one arbitrary complex constant in the solution. This is not the case for equation (A.2), since $h^{(n-1)}(\zeta)$ must satisty condition (2.7ii) which ensures that the unit circle is mapped conformally onto the fluid region. It follows that the solution for $h^{(n)}$ is unique, even though it is not necessary to specify $h^{(n)}$ at any point in $|\zeta| < 1$.

ACKNOWLEDGMENTS

The authors thank Dr. J. R. Ockendon and Dr. A. A. Lacey for their interest and helpful comments. One of us (S.D.H.) also wishes to acknowledge financial support from the United Kingdom Science and Engineering Research Council during the preparation of this paper. The work of the other author (J.M.A.) was supported by a Central Electricity Generating Board Research Fellowship, which is gratefully acknowledged.

REFERENCES

1. P. K. BANNERJEE AND R. BUTTERFIELD, "Boundary Element Methods in Engineering Science," McGraw–Hill, New York, 1981.
2. J. BEAR, "Dynamics of Fluids in Porous Media," Elsevier, New York, 1972.
3. G. F. CARRIER, M. KROOK AND C. E. PEARSON,"Functions of a Complex Variable," McGraw–Hill, New York, 1966.
4. C. M. ELLIOTT AND V. JANOVSKY, *Proc. R. Soc. Edinburgh Sect. A Math.* **88** (1981), 93.
5. C. M. ELLIOTT AND V. JANOVSKY, *in* "MAFELAP 1978" (J. R. Whiteman, Ed.), Academic Press, New York/London 1979.
6. P. HENRICI, *SIAM Rev.* **21** (1979), 481.
7. S. D. HOWISON, A. A. LACEY AND J. R. OCKENDON, *Q.J.M.A.M.*, (1985).
8. J. W. MACLEAN AND P. G. SAFFMAN, *J. Fluid Mech.* **102** (1981), 455.
9. J. A. MCGEOUGH, "Principles of Electro-Chemical Machining," Chapman & Hall, London, 1974.
10. J. C. S. MENG AND J. A. L. THOMSON, *J. Fluid Mech.* **84** (1978), 432.
11. R. MENIKOFF AND C. ZEMACH, *J. Comput. Phys.* **51** (1983), 26.
12. G. H. MEYER, *J. Comput. Phys.* **44** (1981), 262.
13. Z. NEHARI, "Conformal Mapping," Dover, New York, 1952.
14. S. RICHARDSON, *J. Fluid. Mech.* **56** (1972), 609.
15. L. ROMERO, Ph. D. thesis, California Institute of Technology, Pasadena, 1982.
16. P. G. SAFFMAN, *Quart. J. Appl. Math.* **12** (1959), 146.
17. P. G. SAFFMAN AND G. I. TAYLOR, *Proc. R. Soc. London Ser. A* **245** (1958), 312.